A&A 454, 341–348 (2006)
DOI: 10.1051/0004-6361:20065021


Astronomy & Astrophysics

# Bisectors of the cross-correlation function applied to stellar spectra⋆,⋆⋆

## Discriminating stellar activity, oscillations and planets

T. H. Dall[1], N. C. Santos[2,3], T. Arentoft[4], T. R. Bedding[5], and H. Kjeldsen[4]

[1] European Southern Observatory, Casilla 19001, Santiago 19, Chile
e-mail: tdall@eso.org
[2] Centro de Astronomia e Astrofísica da Universidade de Lisboa, Observatório Astronómico de Lisboa, Tapada da Ajuda, 1349-018 Lisboa, Portugal
[3] Observatoire de Genève, 51 Ch. des Maillettes, 1290 Sauverny, Switzerland
[4] Department of Physics and Astronomy, University of Aarhus, 8000 Aarhus C, Denmark
[5] School of Physics, University of Sydney, Sydney, NSW 2006, Australia

Received 14 February 2006 / Accepted 10 April 2006

**ABSTRACT**

*Context.* Bisectors of strong, single spectral lines, usually the Fe I 6252 line, have traditionally been used to examine the velocity fields in stellar atmospheres. This requires high *S/N* often achieved by summing many individual spectra.
*Aims.* We investigate whether bisectors derived from cross-correlation functions (CCF) of single-exposure spectra can be used to provide information on stellar atmospheres, and whether they can be used to discriminate between radial velocity changes caused by planets, magnetic activity and oscillations.
*Methods.* Using a sample of bright stars observed with the HARPS spectrograph, we examine the shapes of the bisectors of individual strong spectral lines in summed spectra, comparing with similar studies in the literature. Moreover, we examine four different quantitative CCF bisector measures for correlations with radial velocity and stellar parameters.
*Results.* We show that CCF bisector measures can be used for quantitative analysis, employing both the absolute values and the variations. From absolute values, $\log g$ and absolute magnitude can be approximated, and from the correlations with radial velocity one can distinguish between magnetic activity, oscillations and orbiting planets as the probable cause of radial velocity variations. We confirm that different isolated spectral lines show different bisector shapes, even between lines of the same element, calling for caution in trying to derive global stellar properties from the bisector of a CCF. For the active star HR 1362 we suggest from the bisector shape an extra photospheric heating caused by the chromosphere of several hundred degrees. We confirm the fill-in of spectral lines of the Sun taken on the daylight sky caused by Rayleigh-Brillouin and aerosol scattering, and we show for the first time that the fill-in has an asymmetric component.

**Key words.** instrumentation: spectrographs – techniques: radial velocities – line: profiles – stars: atmospheres – stars: planetary systems – stars: activity

## 1. Introduction

The analysis of high-resolution stellar spectra can reveal a wealth of information about the physical conditions in the atmosphere. Immediate information on effective temperature, gravity and elemental abundances comes from the analysis of line depths and equivalent widths (EW), while information on the granulation and its cause, the convection, is harder to interpret in terms of line profile variations. These variations are often described in terms of the line bisector. The physical interpretation of the line asymmetries giving rise to the different bisector shapes has been discussed by Gray (2005) from an observational point of view, while theoretical modelling has been done by Asplund et al. (2000) with good results for the Sun.

The bisector has diagnostic power for a number of stellar parameters: The effective temperature and luminosity can be read from the shape of the bisector (the classical "C" shape) and from the height of the blue-most point on the bisector, respectively (Gray 2005). Changes in the bisector shape may have several different causes: Variations at a very low level can be introduced by reflected light from an orbiting planet (Hatzes et al. 1998). More importantly, the bisector is heavily affected by photospheric magnetic fields, and as such it has been used to distinguish radial velocity (RV) changes caused by planets from changes in the photospheric velocity fields induced by magnetic activity (e.g. Queloz et al. 2001). The bisector has been used to infer the presence of unseen stellar companions, both physically connected companions as well as unrelated objects along the line of sight (e.g. Santos et al. 2002; Torres et al. 2005, respectively). Classical stellar oscillations also introduce spectral line asymmetries that will be visible in the bisector, but rather than the

⋆ Based on observations collected at the La Silla Observatory, ESO (Chile), with the HARPS spectrograph at the ESO 3.6 m telescope (ESO Programme 075.D-0760), and on observations obtained from the ESO/ST-ECF Science Archive Facility (ESO Programmes 073.D-0578, 073.C-0784 and 074.D-0380).

⋆⋆ Appendix A only available in electronic form at http://www.edpsciences.org

traditional bisector, other measures have often been used for oscillation studies (e.g. Baldry & Bedding 2000; Dall & Frandsen 2002).

High precision single-line bisector studies require very high *S/N* ratios, which for bright stars can be achieved with a single exposure. For fainter stars, or if the instrument does not offer sufficiently high *S/N* in one exposure, the high *S/N* is often achieved by summation of several tens to hundreds of individual spectra. If the summation is done with spectra taken over a long period of time, it may introduce errors due to developments in the atmosphere (e.g. oscillations or activity) and due to errors on the wavelength calibration of individual spectra. Even small wavelength offsets will have an impact on the summed spectral line and its bisector. This is also true for the case where bisectors are calculated for many different lines in a single exposure and then averaged, since the absolute positions of the individual bisectors are generally not known with very high precision.

The recent advent of a new generation of ultra-stable high-resolution spectrographs has caused a revolution in the detection of extra-solar planets in the past few years. Since the first detection of an extra-solar planet around a solar-like star (51 Peg, Mayor & Queloz 1995), the art of detecting planets by measuring RV displacements has been steadily refined. The methods used are the self-calibration with an iodine cell and the simultaneous ThAr calibration method. While the former is self-calibrated due to the passing of the stellar light through iodine vapor, the second relies on the recording of a ThAr calibration spectrum alongside the stellar spectrum. The simultaneous ThAr method has the advantage that the stellar spectrum is undisturbed, while the iodine-cell introduces hundreds of $I_2$ absorption lines in the spectrum. On the other hand, the ThAr method imposes much stricter requirements on the mechanical stability of the spectrograph. The current state-of-the-art instrument for accurate RV measurements using the simultaneous ThAr method is beyond doubt the ultra-stable spectrograph HARPS (Mayor et al. 2003), installed at the 3.6 m telescope at the La Silla site of the European Southern Observatory, which can achieve precision better than 1 m s$^{-1}$ per exposure (Rupprecht et al. 2004). The high precision of HARPS comes from the high internal mechanical, temperature and pressure stability, combined with the use of the simultaneous recording of a ThAr calibration lamp spectrum alongside the stellar spectrum. In the reduction process, the calibrated spectrum is cross-correlated with an appropriate stellar mask, matched to the spectral type of the target star. The resulting cross-correlation function (CCF) can be thought of as a "mean" spectral line, and as such, it has inherently high *S/N*. Iodine cell spectra have also been used for CCF bisector analysis by Martínez Fiorenzano et al. (2005) after proper removal of the iodine lines. However, this implies an extra reduction step, and in what follows we will only consider CCF's obtained with the simultaneous ThAr method. Due to the high spectral stability, calibration errors are negligible, and errors due to changes with time are eliminated since the CCF is constructed from one single exposure, allowing better time resolution to study variability phenomena. Furthermore, in contrast to the classical bisectors, an absolute velocity position of the HARPS CCF bisector is known to very high precision. On the other hand, combining many different spectral lines, spanning a wide range in wavelength and physical conditions may wash out any physical information, and it does not discriminate between blended and unblended lines. Moreover, the particular mask used in constructing the CCF will have an effect on the shape of the bisector.

In this paper we will investigate the bisectors measured with HARPS on late-type stars. Especially, we will investigate whether the CCF can be used as a meaningful probe of stellar atmospheric physics instead of the classical bisectors of individual spectral lines normally used. In order to do this we compare the classical bisector found from the sum of tens to hundreds of individual spectra with the CCF bisector for a small grid of solar-like stars, both active and non-active.

**Table 1.** The target stars. $N_{sp}$ is the number of 1D spectra combined. The *S/N* was estimated from several continuum regions in the 6200–6600 Å range of the combined spectra. Atmospheric parameters are from Santos et al. (2005) (HR 98, 6585, 7665), Allende Prieto et al. (2004) (Sun, HR 509, 2261, 5933, 7602), Dall et al. (2005a) (HR 1362) and this work (HR 1326, see Sect. 6.3).

| HR | Name | Spec. type | $N_{sp}$ | *S/N* | $T_{eff}$ [K] | log $g$ | [Fe/H] |
|---|---|---|---|---|---|---|---|
| | Sun | G2 V | 628 | 1200 | 5777 | 4.44 | 0.00 |
| 98 | $\beta$ Hyi | G2 IV | 2766 | 1700 | 5837 | 4.00 | −0.08 |
| 509 | $\tau$ Cet | G8 V | 55 | 1500 | 5328 | 4.62 | −0.52 |
| 1326 | $\alpha$ Hor | K1 III | 137 | 800 | 4670 | 2.75 | +0.02 |
| 1362 | EK Eri | G8 III | 9 | 1300 | 5240 | 3.55 | +0.09 |
| 2261 | $\alpha$ Men | G6 V | 36 | 1000 | 5473 | 4.51 | +0.03 |
| 5933 | $\gamma$ Ser | F6 IV | 160 | 1300 | 6246 | 4.30 | −0.15 |
| 6585 | $\mu$ Ara | G3 V | 275 | 1100 | 5806 | 4.28 | +0.32 |
| 7602 | $\beta$ Aql | G8 IV | 135 | 1200 | 5106 | 3.54 | −0.19 |
| 7665 | $\delta$ Pav | G7 IV | 76 | 700 | 5614 | 4.29 | +0.36 |

## 2. Observations and data reduction

The HARPS pipeline (Data Reduction Software, DRS) gives the reduced 1D spectrum plus a file containing the computed CCF for all 72 orders, in addition to the mean CCF, with the computed RV included as a header keyword.

In order to compare the CCF bisector with the classical bisector, we have combined a large number of 1D spectra for each target star (Table 1) in order to reach as high *S/N* as possible. The wavelength calibration and stability of HARPS are good enough that negligible errors are introduced due to the adding of spectra taken on different dates. The observations were obtained during long asteroseismology runs, during planet searches and during technical tests of the guiding system. The solar spectra were taken on the daytime sky for calibration purposes during one of the asteroseismology programmes (Kjeldsen et al., in preparation).

Each individual spectrum was first shifted to the rest wavelength using the calculated RV and the IRAF task `dopcor`, and then combined using `scombine`.

## 3. Bisector definitions and tools

The general definition of the bisector has been given by Gray (1988). In short, one finds the midpoint of the line for a number of intensity positions inside the line. In practice, one may calculate the midpoint between all the points in the blue (red) wing and corresponding interpolated points in the red (blue) wing. For our analysis we interpolate both the red and blue wing in turn, which results in a better sampling of the bisector.

Once the bisector has been found, several parameters can be extracted regarding the shape. Traditionally, the so-called 7%-span or the *velocity span* is used (Toner & Gray 1988). More recently, Gray (2005) found that the height of the blue-most point on the bisector is a powerful luminosity indicator for the cooler spectral types, while the temperature dependence involves

the full shape of the bisector and must be probed by comparing with tabulated values.

Queloz et al. (2001) pioneered the use of bisectors of CCFs. To distinguish between planet- and activity-induced RV variations, they calculated a velocity span, which they note is essentially the inverse slope of the bisector and analogous to the velocity span definition used for classical single-line bisector work. We will reserve the term *velocity span* for classical bisectors, and we will adopt the definition of Queloz et al. of the bisector inverse slope:

$$\mathrm{BIS} = v_\mathrm{t} - v_\mathrm{b}, \quad (1)$$

where $v_\mathrm{t}$ is the mean bisector velocity in the region between 10% and 40% of the line depth, and $v_\mathrm{b}$ is the mean bisector velocity between 55% and 90% of the line depth. This definition is also similar, but not identical, to the velocity span defined by Povich et al. (2001).

While the BIS is a way to quantify the bisector, it is a purely arbitrary measurement. In this paper we will compare the BIS with three other bisector measurements, that are defined as follows: (1) the *bisector slope* $b_\mathrm{b}$, which is defined as the inverse slope from a linear fit to the part of the bisector between 25% and 80% of the line depth. The reason for this choice, is that the CCF bisectors often appear very straight in the central parts, as opposed to the characteristic "C" shape of a classical single-line bisector; (2) the *curvature*, defined as

$$c_\mathrm{b} = (v_3 - v_2) - (v_2 - v_1), \quad (2)$$

which follows Povich et al. (2001), except that we define the mean velocities in segments including 20–30% ($v_1$), 40–55% ($v_2$), and 75–100% ($v_3$) of the line depth. We do not use the velocity displacement $v_\mathrm{b}$ of Povich et al. because it is essentially just an average bisector velocity position, relative to the position of the line core $\lambda_\mathrm{c}$. However, this normalization is purely arbitrary. A better choice would be to measure it relative to the line center i.e. the RV, which in general does not correspond to the line core position. Instead we employ (3) the *bisector bottom* $v_\mathrm{bot}$, which is simply the average of the bottom four points on the bisector minus the RV. This is indeed as arbitrary a construction as any, and can only be justified by considering that we know the absolute position of the line (the RV) to very high precision.

Here we must define what we mean by the absolute position of the line: While the true (in an absolute sense) value of the RV is not known, we can measure absolute positions relative to the instrument zeropoint, which is given with 1 m s$^{-1}$ precision in this case, defined by the long-term stability of the HARPS spectrograph. This precision depends on the *S/N*, so for individual lines it will be somewhat lower than for the CCF.

## 4. Bisectors of single lines

The bisectors of the Fe I $\lambda$ 6252 line are plotted in Fig. 1. Error bars are estimated from the measured *S/N* in the spectra, using the formula of Gray (1988). This is the only line used by Gray (2005), and comparing the stars we have in common ($\beta$ Aql, $\tau$ Cet and the Sun) we find very good overall agreement. Hence HARPS can – not surprisingly – be used as a classical high-resolution spectrograph for line-profile analysis, although it is necessary to sum several individual HARPS spectra to reach the high *S/N*.

Although in an overall sense, the bisector shapes can be understood in terms of simple temperature and luminosity effects, there are aspects of the bisectors in Fig. 1 that call for attention,

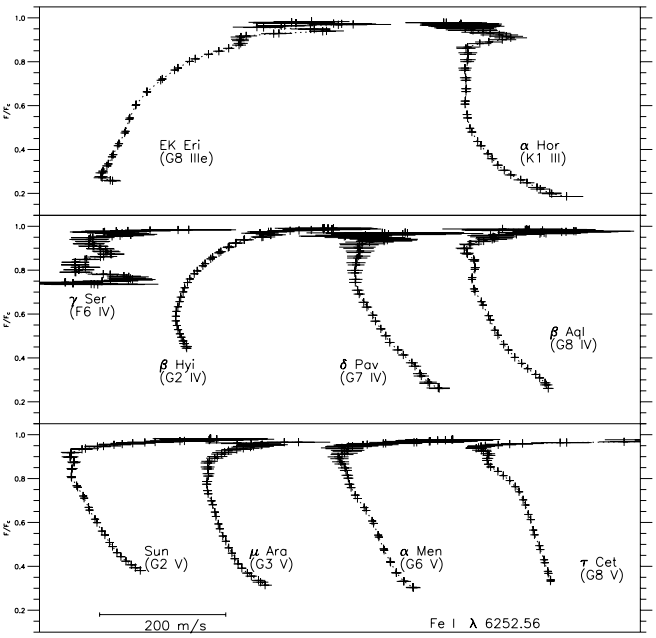


**Fig. 1.** The Fe I $\lambda$ 6252 bisectors of all program stars. Crosses show the calculated points of the bisector with error bars on the velocity.

in particular the peculiar appearance of the $\gamma$ Ser bisector, and the shape of the EK Eri bisector.

As can be seen, the Fe I 6252 line is quite weak in $\gamma$ Ser. Moreover, the lines are broadened by rotation, which further reduces the depth of the line, but on the other hand allows a better sampling of the profile. However, the star is close to the granulation boundary so no definite conclusions can be made.

EK Eri is a well-known over-active but slowly rotating star, exhibiting long-period photometric and spectroscopic variations due to rotational modulation of starspots (Stępień 1993; Strassmeier et al. 1999; Dall et al. 2005a). The bisector does not much resemble the "canonical" shape of a G8 giant (e.g. $\eta$ Dra from Gray 2005, Fig. 3), but rather indicates a somewhat hotter spectral type, especially towards the line core. Since the core is formed in the higher atmospheric layers, this could indicate a substantial heating of the upper layers by the chromospheric activity. Fitting the bisector to the tabulated ones of Gray, we find that the lower part is better described by a G5 star of luminosity class III or II (no perfect fit can be obtained), indicating a heating of the upper layers of the photosphere by ~200–900 K. This is however quite speculative. Since the star is known to have spots, the bisector shape may be reflecting the contributions of different velocity fields in the spots. It could also simply have a misclassified spectral type.

We will now proceed to an investigation of other potentially useful isolated spectral lines (Table 2). These lines were chosen based on VALD linelists (Kupka et al. 1999) of the solar spectrum[1], by requiring that they be unblended, isolated and reasonably strong. The bisectors of the Ca I 6499 line were found to be very irregular for all our sample stars, although no obvious blends could be identified, and they are not plotted. The bisectors of the remaining lines are shown in the figures in Appendix A.

The Fe I $\lambda$ 6151.62 line is very well defined, but not very deep in all our stars. The line may be influenced by weak contributions of Ni I $\lambda$6151.67. The closest major line however,

[1] The Vienna Atomic Line Database, `http://ams.astro.univie.ac.at/vald/`

**Table 2.** All individual spectral lines investigated.

| Line | | $\chi$ [eV] | Notes |
|---|---|---|---|
| Fe I | 6151.62 | 2.17 | Fig. A.1 |
| Fe I | 6252.56 | 2.40 | Fig. 1, (1) |
| Ca I | 6499.65 | 2.52 | (2) |
| Ni I | 6643.63 | 1.67 | Fig. A.2 |
| Fe I | 6750.15 | 2.42 | Fig. A.3 |
| Ni I | 6767.76 | 1.82 | Fig. A.4 |

(1): The "standard" bisector line; (2): strong blending evident in bisector, not plotted.

is more than 0.5 Å away (Si I $\lambda$6152.29). Examining Fig. A.1 we find no obvious systematics, and we consider this line inappropriate for stand-alone analysis. This seems to indicate, that the presence of even very weak blends can disturb the interpretation of the bisector, provided the lines are sufficiently close in wavelength.

The Fe I $\lambda$6252.56 is the standard bisector line, thought to be sufficiently well isolated and free of blends. For low rotational broadenings, the neighboring V I $\lambda$6251.83 line is well separated, and the only other weak lines that may possibly contribute are all on the order of 0.5 Å away or further, namely Ru I $\lambda$6252.07, and Cr I $\lambda$6253.17.

As mentioned, the bisectors of Ca I $\lambda$6499.65 were all very irregular. This may be ascribed to blending with nearby Si I $\lambda$6499.23 and N I 6499.51.

The Ni I $\lambda$ 6643.63 line is very deep and well defined for most of our stars, and generally shows a larger velocity span than the Fe I 6252 line. It is probably affected by blending with V I $\lambda$6643.79 and Gd I $\lambda$6643.94 on the red side and with Sr I $\lambda$6643.53 and Cr I $\lambda$6643.23 on the blue side, which may contribute to the larger velocity span, but rendering any physical interpretations very uncertain.

For the Fe I $\lambda$ 6750.15 line, only a few of our stars show bisectors that resemble the classical "C" shape (Fig. A.3). The line and bisector are well defined, but the sharp redward turn in the upper part may indicate blending with another line. The prime candidates for blending are Fe I $\lambda$6750.58 and Cu I $\lambda$6749.65, although the latter is probably too far away.

The Ni I $\lambda$ 6767.76 line show well defined bisectors for most stars (Fig. A.4). However, no obvious systematics in the shape makes it unlikely that this line can be used to infer atmospheric parameters. It is probably disturbed by Fe I $\lambda$6767.71, and possibly by Co I $\lambda$6768.17.

In conclusion, it seems that a "well-isolated line" translates to a minimum wavelength separation to potential blends of ~0.5 Å.

## 5. CCF bisectors

It was shown by Gray (2005) that the blue-most point of the classical single-line bisector is a very good indicator of luminosity class for the late G to early K stars. If an analogous relationship exists for the CCF bisector, then it will provide us with a luminosity estimate for stars where high-*S/N* spectroscopy is not feasible.

The mean CCF bisectors are plotted in Fig. 2. Their appearances differ somewhat from the Fe I 6252 bisectors, which is not surprising given that they are the bisectors of a "mean" spectral line, and given the diversity of individual line bisectors evident from Figs. A.1–A.4.

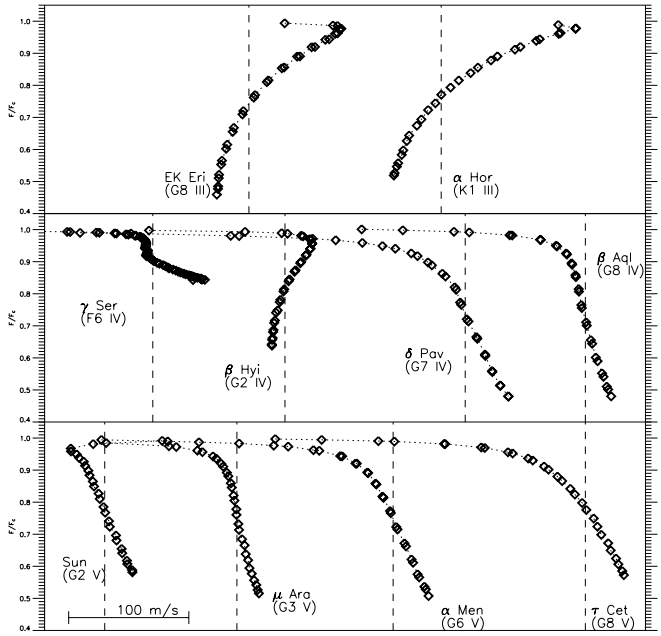


**Fig. 2.** The mean CCF bisectors of all program stars, grouped according to luminosity class. The vertical dashed lines indicate the RV of each star. Formal error bars are the size of the plotting symbols or smaller.

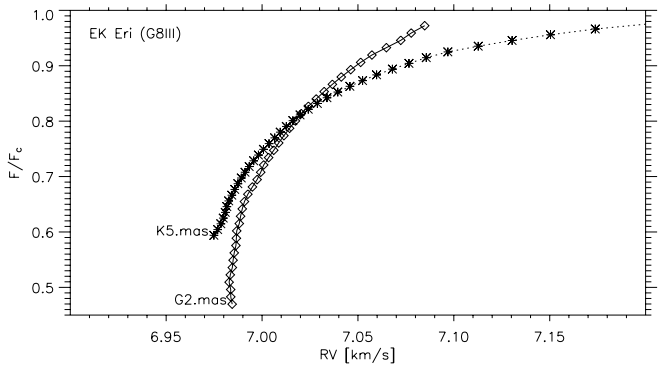


**Fig. 3.** The CCF bisector of EK Eri computed using two different masks.

It must be stressed that one must be careful in comparing CCF bisectors of stars with different spectral types, since the bisector will depend heavily on the mask used in computing the CCF. An example of this is shown in Fig. 3 for EK Eri, using G2 and K5 masks. Hence, one would suspect that in general the CCF bisectors can only be used to compare stars of similar spectral types, with CCFs computed using the same mask. However, as we use a G2 mask to calculate the CCF for all stars except $\alpha$ Hor, this precaution is of less importance in the present study. Another concern about the masks, is whether they are constructed in a way that optimises the physical interpretation of the CCF bisector. These masks are constructed to yield the best possible RV precision, which means excluding very weak, very strong, and heavily blended lines. So while a given mask will include lines of many different elements, it will be free from strong blends and hence represent a near-optimal "average" spectral line.

Returning to Fig. 2, there seem to be trends in the bisector shapes, possibly with temperature, but most noticeably with luminosity and/or gravity. In Fig. 4 we plot the absolute magnitude as a function of BIS + $c_b$, which seem to exhibit a well-defined

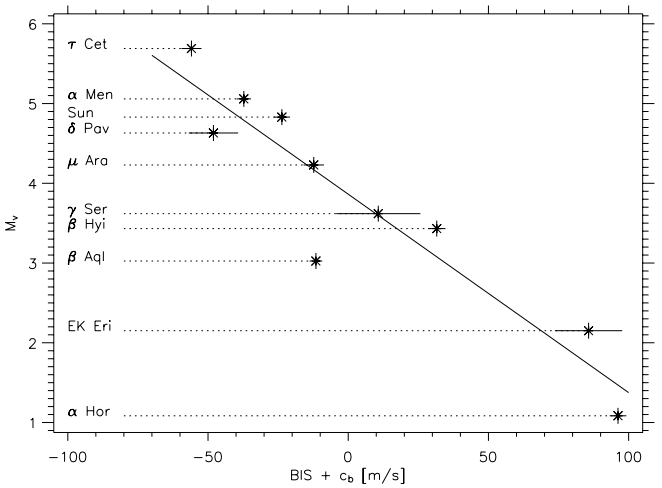


**Fig. 4.** Absolute magnitude as a function of BIS + $c_b$.

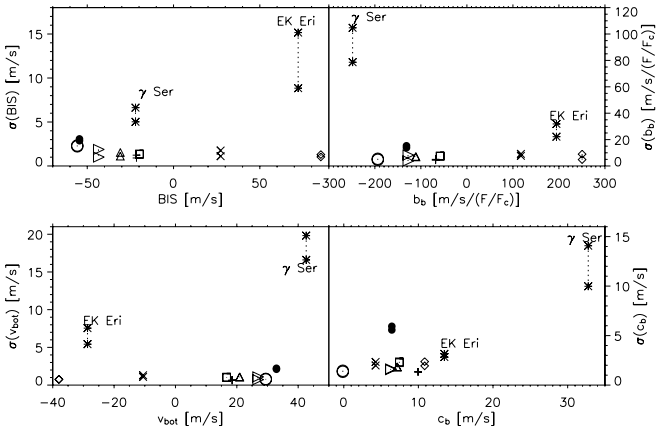


**Fig. 5.** The scatter in all four bisector measures for all program stars. Note that $\gamma$ Ser is close to the granulation boundary, and EK Eri is an active star (discussed in the text). The other symbols are for $\tau$ Cet (◯), Sun (△), $\beta$ Aql (+), $\mu$ Ara (□), $\beta$ Hyi (×), $\delta$ Pav (•), $\alpha$ Men (▷) and $\alpha$ Hor (◇). The individual $1\sigma$ rms scatter (upper point) and point-to-point scatter (lower point) are connected with dotted lines.

linear relationship. A similar relationship is found plotting $\log g$ versus BIS + $c_b$. We derive the approximate relations

$$M_v = 3.86 - 24.88(\mathrm{BIS} + c_b) \quad (3)$$

$$\log g = 4.06 - 9.22(\mathrm{BIS} + c_b), \quad (4)$$

which we must stress are only approximate, are based on very few data points, and should not be used to derive final stellar parameters.

If proven to be correct, these relationships can be used to measure the luminosity from the shape of the average CCF bisector, in analogy with the blue-most point luminosity indicator for the classical bisector, only that these relationships may be extendable to all the late spectral types. However, to establish a reliable relationship, or indeed to determine whether such a relationship exists at all, more data is needed. Obviously, the fact that the values of the bisector measures depends on the mask used, calls for extreme caution. A more thorough analysis of a larger sample is currently in progress (Dall et al., in preparation).

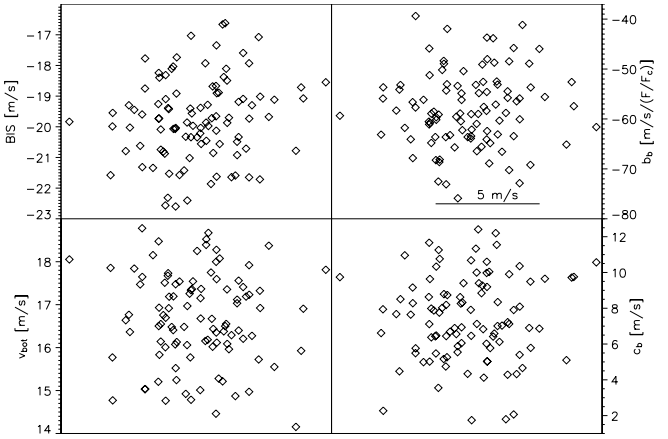


**Fig. 6.** The bisector measures as functions of RV for $\mu$ Ara. The scatter is dominated by solar-like $p$-mode oscillations; see text. Horizontal axis is RV in all plots, with the scale indicated in the upper right panel.

## 6. Variations of CCF bisectors

In the remainder of this paper we will concentrate on the changes in the CCF bisector measures, rather than the absolute values of these, and examine how these changes may be used as diagnostic tools when looking at only one star. In doing so, the dependence on the mask used for the CCF disappears, as we look only at relative changes.

First, however, we must address the expected scatter of the measures in the case where no activity or oscillations are likely to show up, using the non-active stars with low-amplitude oscillations, i.e. primarily $\mu$ Ara and the Sun. Some of the remaining targets will then be addressed in turn.

A general idea of the expected scatter can be gained by looking at Fig. 5, which shows the scatter in the bisector measures for all the stars. Obviously, the noise will depend on the *S/N* of the CCF and on the spectral type. As can be seen, except for $\gamma$ Ser and EK Eri, the scatter is very similar over the full range of spectral and luminosity classes. In particular, the RMS spread and the point-to-point scatter are almost identical.

### 6.1. No correlations – $\mu$ Ara

$\mu$ Ara is the host of a low-mass planet orbiting the parent star in 9.5 days (Santos et al. 2004). Moreover, it exhibits well-described low-amplitude solar-like $p$-mode oscillations with individual mode amplitudes up to 0.4 m s$^{-1}$ (Bouchy et al. 2005; Bazot et al. 2005). From the ESO Science Archive we retrieved 100 consecutive CCF observations, spanning 3.7 h – long enough to include several oscillation cycles and short enough to avoid longer-term effects from the presence of the planet.

The four investigated bisector measures are shown in Fig. 6. The ∼10 m s$^{-1}$ scatter in RV (horizontal axis) is dominated by the $p$-mode oscillations. Note that the measured velocity is a sum of a few dozen modes, each of which has small (∼0.4 m s$^{-1}$) amplitude. These modes beat to produce the observed peak-to-peak velocity excursions (see e.g. Bouchy et al. 2005, Fig. 5). It is evident that no obvious correlations are present, and we will then adopt the scatter shown in these plots to be "typical" of non-correlating bisector measures.

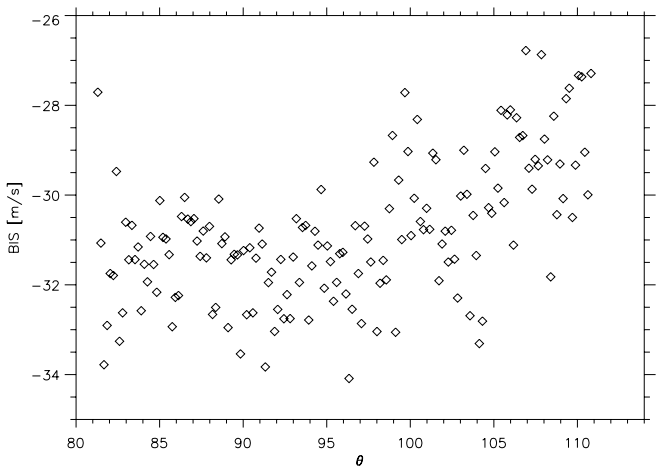


**Fig. 7.** The Sun: the bisector measure BIS as function of the angular distance to the sun $\theta$ for one 2.6 h segment. The same trend is observed in $b_b$, while no such trends can be seen for $v_{bot}$ and $c_b$.

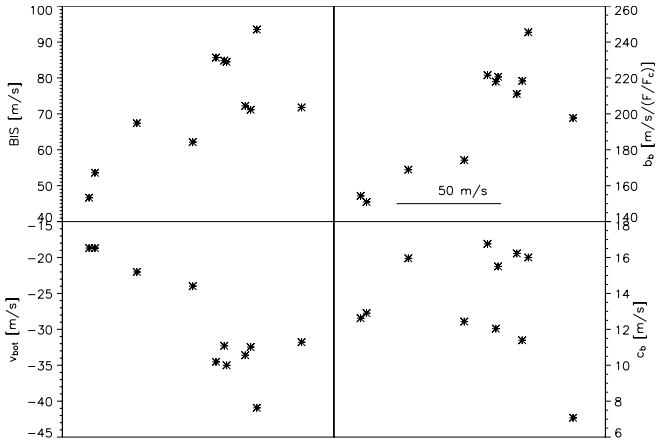


**Fig. 8.** The bisector measures for EK Eri. Horizontal axis is RV in all plots, with the scale indicated in the upper right panel.

### 6.2. Scattering of sunlight in the Earth atmosphere

The spectral lines in solar spectra obtained on the daytime sky are known to exhibit EW and line depth changes. Gray et al. (2000) measured the line depth variations and found them to be symmetrical, i.e., they found no changes in the bisector due to asymmetries of the lines, as a function of the angular separation $\theta$ between the telescope pointing and the position of the Sun. Their detection limit on the bisector variations was 20 m s$^{-1}$, and they mention the possibility of smaller variations being present. They successfully modeled the line depth variations in terms of aerosol and Rayleigh-Brillouin scattering as a function of $\theta$.

Our data, taken in directions close to opposite the sun, covers a span in $\theta$ of ∼30°, in which we observe a smooth change in the CCF line depth on the order of 1%, consistent with the findings of Gray et al. (2000). From our data it is evident that there is an asymmetric contribution to the atmospheric scattering, as revealed in the BIS, which varies with 4 m s$^{-1}$ over the interval (Fig. 7). Obviously, a better sampling of $\theta$ from 0° to 180° would be desirable, as we demonstrate that line asymmetries in the scattering can indeed be detected with HARPS.

### 6.3. Variations due to oscillations?

The stars $\alpha$ Men, $\delta$ Pav, $\beta$ Hyi and $\alpha$ Hor are all expected to show solar-like $p$-mode acoustic oscillations (see Kjeldsen et al. 2005, for $\delta$ Pav and $\beta$ Hyi).

Our data on $\alpha$ Men were taken in individual six-spectra segments of less than one hour duration, over a period of three months. Peak-to-peak variation is ∼6 m s$^{-1}$, and no correlation with bisector measures can be seen.

The observations of $\delta$ Pav span 1.8 hours, and show clear solar-like oscillations with peak-to-peak amplitudes of ∼10 m s$^{-1}$. No correlation with bisector measures can be seen. Higher scatter of the bisector measures compared with the other stars is evident from Fig. 5. We have no explanation of this fact other than the bad weather conditions (bad seeing and wind from the south) prevailing at the time of observation. This, and the short exposure times, could also be part of the reason for the low *S/N* in the combined spectrum.

The results of the asteroseismic campaign on $\beta$ Hyi will be published elsewhere (Kjeldsen et al., in preparation). Here it suffice to note the peak-to-peak amplitude of the $\beta$ Hyi oscillations of up to ∼10 m s$^{-1}$, revealing weak correlations with bisector measures BIS and $b_b$. A Fourier analysis of the bisector measures reveals that the oscillation signal is clearly present in the BIS and $b_b$ data, while $v_{bot}$ and $c_b$ do not reveal any oscillation signal at the $6\sigma$ level. This could indicate that the upper part of the line is insensitive to the oscillations.

$\alpha$ Hor is one of the most stable Hipparcos stars, with a photometric error of <0.3 mmag (Adelman 2001). No reliable stellar atmospheric parameters could be found in the literature, so we performed an ATLAS9 (Kurucz 1993) model atmosphere fitting using Fe I/Fe II ion balance, following the procedure of Dall et al. (2005b). The RV curve of $\alpha$ Hor shows a smooth variation over the duration (∼2.5 h) of the observations. The peak-to-peak amplitude is ∼25 m s$^{-1}$, maybe slightly larger as we have not covered the full period. Assuming this to be due to stellar oscillations, using the scaling relation of Kjeldsen & Bedding (1995) predicts a photometric amplitude of ∼0.3 mmag, i.e. the oscillations should have been barely detectable by Hipparcos. More importantly for our purpose, variations at this level cannot be seen in the bisector.

In summary, solar-like $p$-mode oscillations have a weak influence on the bisector, and are only properly revealed by a Fourier analysis.

### 6.4. Variations due to activity

The star EK Eri shows a clear example of activity induced bisector variations. The activity and associated variability of EK Eri has been studied extensively for years, and it is generally agreed to be a slow rotator with a fossil Ap-type magnetic field (Stępień 1993; Strassmeier et al. 1999). Dall et al. (2005a) found the BIS of the CCF to correlate well with the RV and the activity index $\log R'_{HK}$, meaning that the activity displays a coherent pattern from the photosphere to the chromosphere.

We examined all four bisector measures, shown in Fig. 8, in order to test which is best suited to describe activity induced RV changes. In addition to the BIS, $b_b$ and $v_{bot}$ show clear correlations with the RV, while $c_b$ seem to be insensitive to the activity, which is also evident from Fig. 5. Hence, it seems that the stability of $c_b$ is real, and that the curvature of the CCF bisector is unaffected by activity. Note that the slopes of the correlations are positive for BIS and $b_b$ as expected from activity and negative for $v_{bot}$, and that the peak-to-peak amplitude is of the order ∼100 m s$^{-1}$, i.e., much higher than the oscillation scatter.

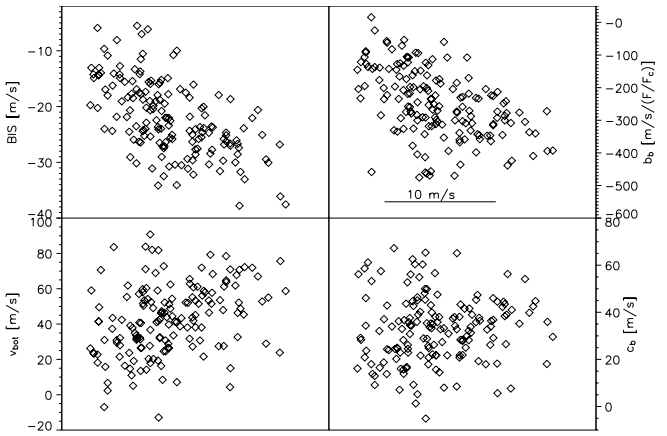


**Fig. 9.** The bisector measures as functions of RV for $\gamma$ Ser. Horizontal axis is RV in all plots, with the scale indicated in the upper right panel.

### 6.5. Variations due to unseen companion?

For $\gamma$ Ser, the scatter in all the bisector measures are high (Fig. 5). A closer inspection reveals clear correlations with BIS and $b_b$, less clear with $v_{bot}$ and no correlation with $c_b$ (Fig. 9). Note that the slopes of the correlations are opposite to the case of the activity induced variation of EK Eri. This hints that the variation may be due to either a fainter orbiting star or a chance-alignment with a background star, corresponding to the case of HD 41004 (Santos et al. 2002) where the blending with light from a much fainter companion produced a negative slope of BIS versus RV. Such a correlation could also result from chance alignment with a fainter background star, modulated by seeing variations. Note that the possible companion discussed here is a *stellar* companion, contributing flux to the total spectrum. A planetary companion would not show up in this way.

We hesitate to propose that the correlations could be due directly to oscillations, since the apparent amplitude of the RV variation is lower than for $\alpha$ Hor, where no correlations were found, and similar to $\beta$ Hyi, where only weak correlations were found. However, the slope of the correlations are the same as for $\beta$ Hyi, so this may actually reflect oscillations, and the reason for it showing up in $\gamma$ Ser and not in $\alpha$ Hor may lie in the proximity of the former to the granulation boundary. This question must be resolved by observing a larger sample of stars.

## 7. Concluding remarks

In this paper we have examined a small sample of well-studied bright stars of different spectral types and luminosity classes. We have measured the bisectors of isolated spectral lines using high *S/N* combined spectra, and we have measured bisectors of CCFs of individual exposures, obtaining a high *S/N* from the combination of hundreds of individual lines.

The main purpose of this paper – to relate the single-line classical bisector to the single-spectrum combined-line CCF bisector – has been achieved: We have shown that one may use the CCF bisector in much the same way as one would use the single-line bisector. Moreover, we have shown that it is possible to use the defined CCF bisector measures for quantitative analysis, employing both the absolute values and the variations.

For the single-line classical bisectors, we can point out the following:

- We confirm the general shapes of the bisectors of the Fe I 6252 line for stars of different spectral and luminosity classes, as published by Gray (2005), using sums of HARPS spectra to achieve high *S/N*. We did not find other spectral lines with similar well-behaved bisector patterns with spectral type. We find that to be well isolated, a line must not have any potential blends closer than ∼0.5 Å, based on the six lines we have investigated.
- Based on the bisector shape of the Fe I 6252 line in the spectrum of EK Eri, we suggest that this may point to an extra heating of the upper photosphere of several hundreds degrees, presumably supplied by the active chromosphere. However, the peculiar bisector shape may also be due to photospheric spots, or to inaccurate spectral classification.

For the CCF bisectors, we can point out the following:

- We find that the CCF bisector could be used to approximate the luminosity and $\log g$ using the absolute values of the bisector measures BIS, $b_b$, $v_{bot}$, and $c_b$, and we derive approximate relationships. It is slightly surprising that a luminosity relationship can be recovered in the CCF bisector, since it includes many different spectral lines with different individual bisector shapes, not only between lines of different elements, but between lines of the same element too (Fig. 1 and the Appendix). An added advantage of the CCF bisector in this case, is that the relationship seems to apply to all the spectral types of our sample, and is not dependent on the existence of a blue-most point, which disappears for the hotter stars. Naturally, the validity and accuracy of such relationships will be the subject of future study of a larger sample of stars.
- We find that normal $p$-mode solar-like oscillations do not reveal themselves in the bisectors at a significant level (for peak-to-peak RV amplitudes $<25$ m s$^{-1}$). However, there may be a dependence of the bisector response to oscillations on the spectral type or luminosity class. For $\gamma$ Ser we do find correlations between RV and the bisector measures BIS and $b_b$, even though the oscillations are at a very low level. We speculate that this could be due to an unseen stellar companion, either a physical companion or a chance line-of-sight alignment. Another possibility is that $\gamma$ Ser is too close to the granulation boundary to allow any meaningful interpretation of its bisectors.
- For EK Eri, the only active star of our sample, we find the RV correlated with all bisector measures except the curvature $c_b$. Note that the slopes of the correlations for $\gamma$ Ser and EK Eri are reversed, giving an indication of different mechanisms being involved.

Finally, we confirm the effects of aerosol and Rayleigh-Brillouin scattering on solar spectra taken on the daylight sky. Moreover, we show for the first time that the bisectors and hence the lines change shape, thus there is an asymmetric component of the scattering.

*Acknowledgements.* This research has made use of the SIMBAD database, operated at CDS, Strasbourg, France. Support from Fundação para a Ciência e a Tecnologia (Portugal) to N.C.S. in the form of a scholarship (reference SFRH/BPD/8116/2002) and a grant (reference POCI/CTE-AST/56453/2004) is gratefully acknowledged. Support from The Danish Natural Science Research Council is gratefully acknowledged.

## References

Adelman, S. J. 2001, A&A, 367, 297
Allende Prieto, C., Barklem, P. S., Lambert, D. L., & Cunha, K. 2004, A&A, 420, 183

Asplund, M., Nordlund, Å., Trampedach, R., Allende Prieto, C., & Stein, R. F. 2000, A&A, 359, 729
Baldry, I. K., & Bedding, T. R. 2000, MNRAS, 318, 341
Bazot, M., Vauclair, S., Bouchy, F., & Santos, N. C. 2005, A&A, 440, 615
Bouchy, F., Bazot, M., Santos, N. C., Vauclair, S., & Sosnowska, D. 2005, A&A, 440, 609
Dall, T. H., & Frandsen, S. 2002, A&A, 386, 964
Dall, T. H., Bruntt, H., & Strassmeier, K. G. 2005a, A&A, 444, 573
Dall, T. H., Schmidtobreick, L., Santos, N. C., & Israelian, G. 2005b, A&A, 438, 317
Gray, D. F. 1988, Lectures on spectral-line analysis: F, G, and K stars (Ontario: The Publisher)
Gray, D. F. 2005, PASP, 117, 711
Gray, D. F., Tycner, C., & Brown, K. 2000, PASP, 112, 328
Hatzes, A. P., Cochran, W. D., & Bakker, E. J. 1998, ApJ, 508, 380
Kjeldsen, H., & Bedding, T. R. 1995, A&A, 293, 87
Kjeldsen, H., Bedding, T. R., Butler, R. P., et al. 2005, ApJ, 635, 1281
Kupka, F., Piskunov, N., Ryabchikova, T. A., Stempels, H. C., & Weiss, W. W. 1999, A&AS, 138, 119
Kurucz, R. 1993, ATLAS9 Stellar Atmosphere Programs and 2 km/s grid. Kurucz CD-ROM No. 13, Cambridge, Mass.: Smithsonian Astrophysical Observatory
Martínez Fiorenzano, A. F., Gratton, R. G., Desidera, S., Cosentino, R., & Endl, M. 2005, A&A, 442, 775
Mayor, M., & Queloz, D. 1995, Nature, 378, 355
Mayor, M., Pepe, F., Queloz, D., et al. 2003, The Messenger, 114, 20
Povich, M. S., Giampapa, M. S., Valenti, J. A., et al. 2001, AJ, 121, 1136
Queloz, D., Henry, G. W., Sivan, J. P., et al. 2001, A&A, 379, 279
Rupprecht, G., Pepe, F., Mayor, M., et al. 2004, in Proc. SPIE, 5492, 148
Santos, N. C., Mayor, M., Naef, D., et al. 2002, A&A, 392, 215
Santos, N. C., Bouchy, F., Mayor, M., et al. 2004, A&A, 426, L19
Santos, N. C., Israelian, G., Mayor, M., et al. 2005, A&A, 437, 1127
Stępień, K. 1993, ApJ, 416, 368
Strassmeier, K. G., Stępień, K., Henry, G. W., & Hall, D. S. 1999, A&A, 343, 175
Toner, C. G., & Gray, D. F. 1988, ApJ, 334, 1008
Torres, G., Konacki, M., Sasselov, D. D., & Jha, S. 2005, ApJ, 619, 558

# Online Material

## Appendix A: Bisectors of additional lines

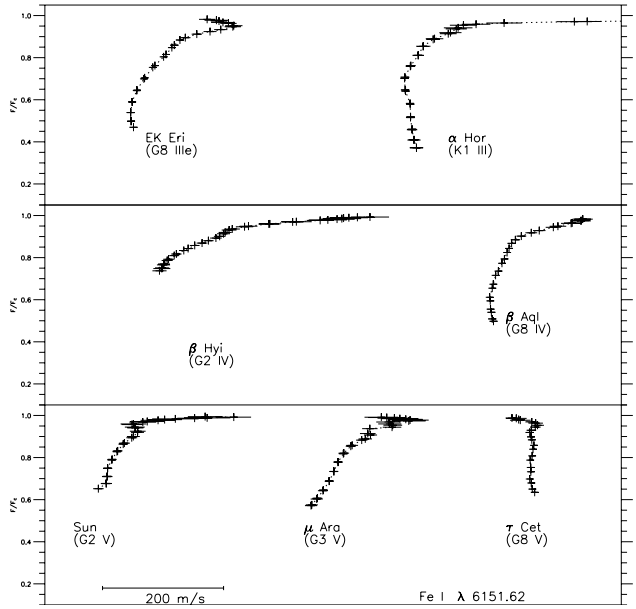


**Fig. A.1.**

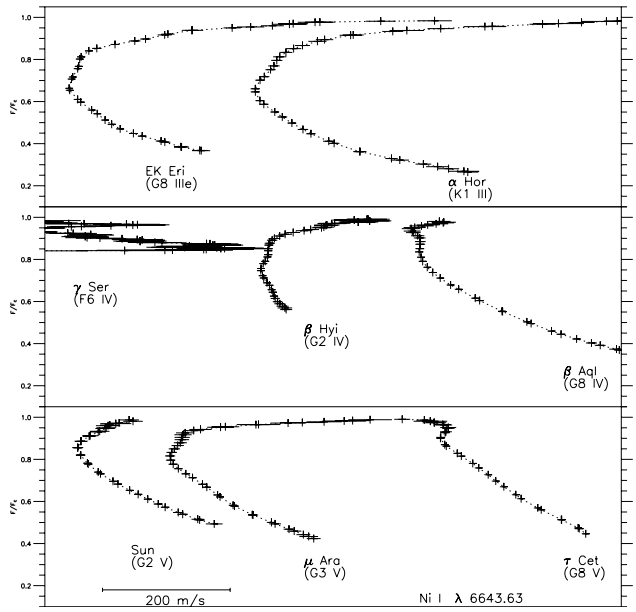


**Fig. A.2.**

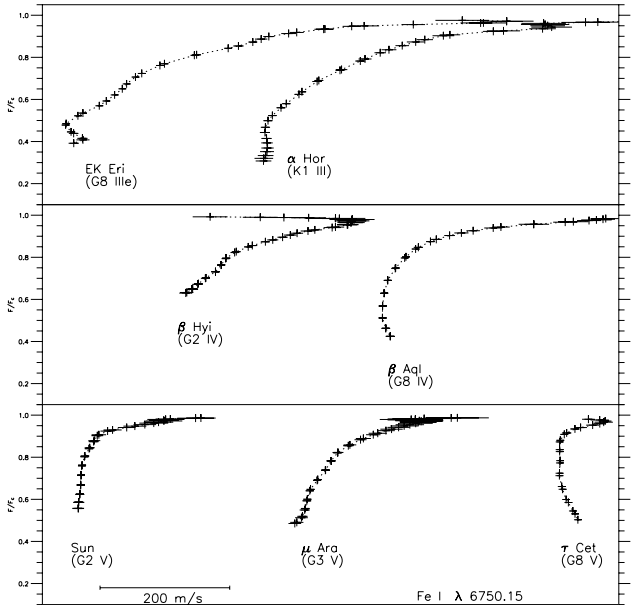


**Fig. A.3.**

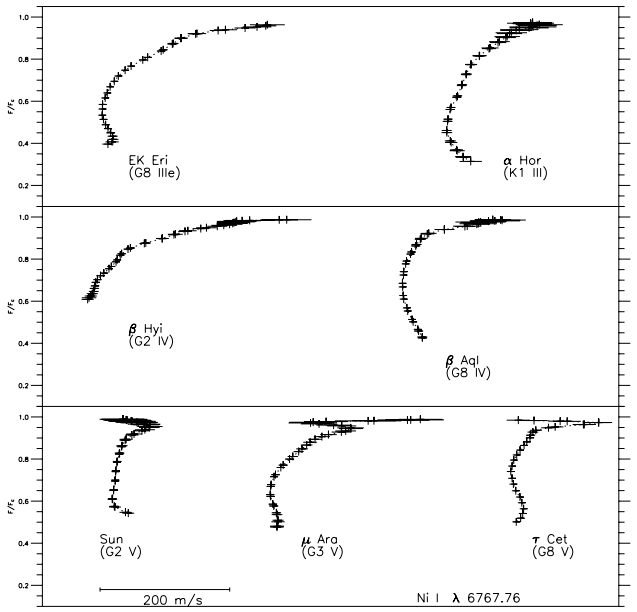


**Fig. A.4.**